Post-print of: M. Martynow, A. Zielińska, M. Marzejon, M. Wojtkowski and K. Komar, "Pupil detection supported by Haar feature based cascade classifier for two-photon vision examinations," 2019 11th International Symposium on Image and Signal Processing and Analysis (ISPA), Dubrovnik, Croatia, 2019, pp. 54-59, doi: 10.1109/ISPA.2019.8868706.

Pupil detection supported by Haar feature based cascade classifier for two-photon vision examinations

Miłosz Martynow
Baltic Institute of Technology
Gdynia, Poland
Faculty of Applied Physics and Mathematics
Gdańsk University of Technology
Gdańsk, Poland
0000-0001-6225-2420

Agnieszka Zielińska
Faculty of Physics, Astronomy and Informatics
Nicolaus Copernicus University
Toruń, Poland
0000-0003-1528-0028

Marcin Marzejon
Institute of Physical Chemistry
Polish Academy of Sciences
Warsaw, Poland
Faculty of Electronics, Telecommunications and Informatics
Gdańsk University of Technology
Gdańsk, Poland
0000-0001-8674-0437

Maciej Wojtkowski
Institute of Physical Chemistry
Polish Academy of Sciences
Warsaw, Poland
Baltic Institute of Technology
Gdynia, Poland
0000-0003-0599-0878

Katarzyna Komar
Faculty of Physics, Astronomy and Informatics
Nicolaus Copernicus University
Toruń, Poland
Baltic Institute of Technology
Gdynia, Poland
0000-0003-0229-3735

***Abstract*—The aim of this paper is to present a novel method, called Adaptive Edge Detection (AED), of extraction of precise pupil edge coordinates from eye image characterized by reflections of external illuminators and laser beams. The method is used for monitoring of pupil size and position during psychophysical tests of two-photon vision performed by dedicated optical set-up. Two-photon vision is a new phenomenon of perception of short-pulsed near infrared laser beams focused on human retina as having color of half of their wavelength and it is caused by two-photon absorption occurring in human photoreceptors during safe illumination conditions. The AED method is constructed of four basic image processing operations of computational complexity of order approx. O(width*height), which makes possible to use it in real time applications. Furthermore, to achieve high resistance of AED method for presence of light reflections on images as well as other difficulties, we apply machine learning model - Haar feature based cascade (Hfbc) classifier. After implementation of trained Hfbc classifier, our method is able to find pupil edge on images, for which it was failed with this before. Finally, we obtain pupil radius and central pixel coordinates even for images containing eyelashes, changed position of illuminator or presence of reflections caused by stimulating laser beam, which significantly improves pupil edge detection efficiency.**

Keywords— biomedical imaging, pupillometry, Haar features, cascade classifier, Suzuki contour detection, pupil dynamics, two-photon vision.

I. Introduction

Image analysis in general is based on mathematical operations on pixel value, which are carried out on the separate pixel or in reference to its neighbors. Due to these basic operations it is possible e.g. blurring the image, binarizing it or edges extracting [1]. All of them do not require any extra data, except additional parameters for filtering function. Machine learning techniques, which are widely developed recently, are different approach to image analysis: depending not only on the analyzed image but also on the big data bases that contain previously prepared and described images. Typical examples are: Convolutional Neural Networks [2], [3] or Haar feature based cascade classifiers (Hfbc classifier) [4], [5]. These well-known methods can be used for detection or classification of any type of described shape in the analyzed image [6], [7]. Combining of both above mentioned approaches may speed up and increase accuracy of image analysis, because it would be possible to find at once all interested shapes and compare found details. Here we propose to apply such combination of both approaches to images of eye pupil registered during psychophysical tests of vision.

Two-photon vision is a new phenomenon of perception of short-pulsed near infrared laser beams focused on human retina. It is based on perception of these beams as having color of half of the laser wavelength. The sensation is caused by two-photon absorption occurring in human photoreceptors during safe illumination conditions [8]. This newly described phenomenon still requires further investigations, which can be performed only by using specially designed optical set-up for forming and deliver two-photon stimulus to human retina [9]. Pupil size and position of its center in regard to optical axis of the instrument are crucial factors directly influencing experimental conditions of psychophysical tests. Therefore, fast and accurate method of automated pupil edge detection is strongly needed for monitoring and tracking pupils throughout experiments. The series of grayscale eye images gathered during typical measurement session are characterized by presence of difficult to avoid reflections of infrared illuminator, as well as stimulating laser beams. The two-

This work was supported by City of Gdynia, project No. 3/DOT/2016, grant 2016/23/B/ST2/00752 funded by National Science Centre, and grant TEAM TECH/2016-3/20 funded by Foundation for Polish Science.

This project has received funding from the European Union's Horizon 2020 research and innovation programme under grant agreement No 666295. Scientific work funded from the financial resources for science in the years 2016-2019 awarded for the implementation of an international co-financed project.

photon stimulus is formed by fast scanning of retina by stimulating laser, so its reflections are not constant on consecutive images. Due to these particular complications we need pupil detection method that will work efficiently under existing circumstances, which are different from typically used in pupillometry.

In this paper we present a novel way developed for extracting pupil shape from eye images registered by specific instrument. Up to date we have collected dataset of more than 90 000 different images of human eyes. Pupil is usually the biggest object on registered picture, therefore we are able to relatively easy extract coordinates of pupil edge pixels and, consequently, other parameters describing pupil and its dynamics. For this purpose we use our own method, Adaptive Edge Detection (AED), consisting of only four basic image operations with algorithmic efficiency $\approx O(width \cdot height)$ i. e. Gaussian Blurring, Adaptive Thresholding, Laplace Edge Extraction and Suzuki Edge Detection [10]. Afterwards, edge coordinates obtained by AED method are used for finding pupil radius and center by least-squares fitting of circle. Additionally, we improved the AED method by adding the Hfbc classifier trained on selected images from our eye pictures dataset. After training, our program was able to manage with deviated images i.e. containing eyelashes, changed position of illuminator or presence of reflections caused by stimulating laser beam.

This paper consists of following sections: II: Related work in field of automated pupil detection; III: Laboratory set-up for two-photon vision measurements; IV: Adaptive Edge Detection method description; V: Description of least squares circle fitting method applied to points of found pupil edge; VI: Improvement of pupil edge pixels detection by Haar feature based cascade classifier; VII: Conclusions.

II. Related work

Analysis of pupil dynamics is useful for many clinical applications. Pupil reaction is controlled by autonomic nervous system, therefore pupillometry gives insight into its function. Optic nerve's damage is routinely tested by observing reaction of both pupils to light, thus accurate measuring of this reaction may help to distinguish between functional from organic visual loss [11]. Injury of the oculosympathetic pathway results in so-called Horner syndrome, which can be also diagnosed by digital pupillometry [12]. Pupillary autonomic neuropathy is considered to be early sign of systemic autonomic neuropathy, which can be caused by type 1 diabetes [13]. Pupils asymmetry sometimes is connected with brain damage [14] therefore it is very important clinical parameter as well as significant deviations from circular shape of one pupil can be caused by intracranial hypertension in patients after brain injuries [15]. Accurate pupillometry can be even applied for functional examinations of vision: e.g. to some extent it may substitute perimetry for Retinitis Pigmentosa patients [16] or examine of rod and cone function in macular dystrophy [17]. Furthermore, pupil behavior analysis is important also for non-medical applications: eye tracking instruments are a part of human-computer interface for military, aviation, augmented reality and systems for helping patients with tetraplegia. Gaze controlled systems used in above applications assign different function to changes in pupil position and blinking [18], [19].

Automated pupillometry has been developed over the last 30 years, therefore many methods for pupil detection exist. However, it is still active field of research, possibly due to large variety of conditions, which may be encoutered during pupil registration: e. g. different illumination types, irregularities between pupils or patients with droopy eyelids and eyelashes partially covering the eye. Method presented by Świrski et al. [5] has been described relatively recently. It uses Hfbc classifier for pupil detection and k-means binary segmentation of histogram of the pupil-only region for automatic level selection for global thresholding. The method effectively finds pupils, even irregular ones, because of concentration on the non-centrally located object. However, due to global thresholding, it may be less effective for images with non-uniform illumination. Another lately proposed methods, both by Fuhl et al., are Exclusive Curve Selector (ExCuSe) [20] and Ellipse Selection (ElS) [21]. First method uses analysis of histogram for detection of intensity peak that is higher than manually selected threshold. If the peak is detected, then further pupil detection steps are performed: Canny Edge detection [22], straight lines filtration, choosing curve line as a pupil proposal and least-squares fitting to ellipse that lies closest to the center. Later method implements Canny Edge detection and fits many ellipses to found edges. Finally, the best fitted one is chosen as a pupil. The newest method for pupil obtaining is called Pupil Reconstructor (PuRe) and was proposed by Santini et al. [23]. It is also based on ellipsis fitting after edges extraction and some additional morphological operations. Referring to the benchmarks presented in the PuRe paper [23], speed and accuracy of detection shows substantial increase for newer algorithms. Speeds of ElS and PuRe method are near to the 120 frames per second, while ExCuSe and Świrski algorithms are half time slower on the same machine. Although all described algorithms are still useful for real time pupil detection, the PuRe algorithm was the most accurate one under testing on the five images datasets [23].

Haar feature based cascade is well-known machine learning technique for visual object detection, presented for the first time in 2001 by Viola and Jones [4]. It was significantly improved in 2002 in the Intel Labs by Lienhart, Kuranov and Pisarevsky [24]. There is a lot of free very well trained Hfbc classifiers over the internet, which are able to detect variety of objects e.g. faces or even eyes, but we didn't find any trained models, which would be suitable for images registered in our two-photon vision system. Hfbc classifier as a machine learning technique requires relatively small amount of positive images to train the weights used in cascade classification. Positive images shows object of interest in different variants. Number of negative images should be approximately twice of the positive ones.

Discussed above methods are able to detect pupils on images where pupil is the darkest and homogenous object. Our laboratory set-up delivers images characterized by presence of reflections of infrared illuminator and stimulating laser beams, thus we decide to develop our own method for extraction of exact pupil edge pixels and, consequently, to pupil detection and analysis. This method is based on the fact, that pupil is the biggest object on our images or on pupil-only region found by Hfbc classifier. The main assumption of our approach was usage of well-known, fast and basic image operations, which are stable, exhibit low algorithmic complexity and fast implementation to different programming environments like Python, C/C++ and LabVIEW.

III. Laboratory set-up for two-photon vision measurements

Laboratory set-up for two-photon vision examination is schematically shown in Fig. 1 and described in detail elsewhere [9]. Briefly, it consists of femtosecond laser emitting fundamental train of pulses of central wavelength 1040 nm, pulse length of 200 fs and repetition frequency 76 MHz and its second harmonic – 520 nm. The laser beams are coupled into single mode fibers (resulting in pulse stretching at fiber output up to over a dozen picoseconds) and delivered to optical set-up, which main optical path consists of: (1) gradient neutral density filter mounted on stepper motor for automated control of optical power of beam transmitted to human eye; (2) power meter for measuring this power; (3) galvanometric scanners optically conjugated with subject's pupil that allows forming of optotypes of different shape and size by fast scanning of subject's retina. Another parts of optical set-up are background/bleaching and fixation optical paths for producing appropriate conditions for particular psychophysical test. For this paper, most important is optical path of pupil camera, which is optically conjugated with subject's pupil plane. The polarizer P and filter F are used to reduce corneal reflections of stimulating laser beam. Nevertheless, because of relatively high intensity and close proximity of wavelength of stimulating IR beam in comparison to infrared illuminator, we are not able to completely avoid of these reflections on gathered images. We also use, depending on examination, different variants of

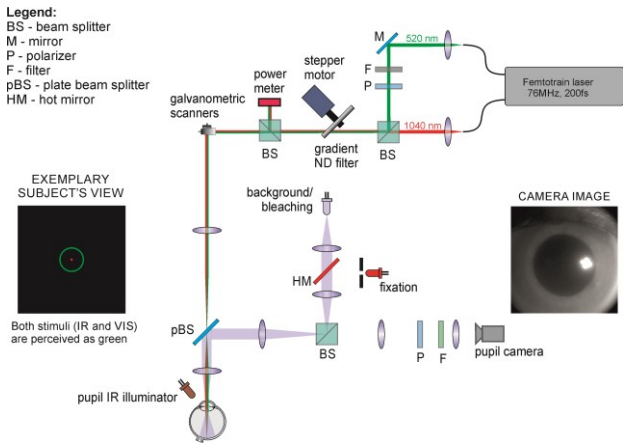

Fig. 1. Optical set-up for two-photon vision examination.

infrared illuminator: the diodes can be placed on the side of the eye or radially on last lens mountings, which cause different shape and positions of illuminator reflections (see Fig. 4).

The set-up operation under different types of psychophysiological tests is controlled by dedicated LabVIEW programs.

IV. Adaptive Edge Detection method

Detection of the pupil edge by AED method is four steps process illustrated in Fig. 2. All steps were obtained by OpenCV 4.0.1 open source library [25], which ensures the quality of methods and provides them as optimized, tested and well-described functions. Another advantage of OpenCV library is that it is available to the number of programming languages e.g. Python 3.6 used in this project or C++14. Analyzed image is a 8-bit grayscale image of both width and height equal to $W = H = 512$. During first three steps we are dealing with convolutional operations given by general equation:

$$g(i,j) = \sum_{k=0}^{K_x} \sum_{l=0}^{K_y} f(i+k, j+l) h(k,l) \qquad (1)$$

where $g(i,j)$ is value of the filtered pixel, $f(i,j)$ is the old pixel value and $h(k,l)$ is window of filtering function. i and j describe currently filtered pixel coordinates under the kernel window coordinates k and l and Kx, Ky define window size.

First step of AED method is Gaussian Blurring, which helps in minimization of effects due to random change of pixel intensity e.g. caused by dust particles. Gaussian type of blurring is most effective for our pupil detection algorithm i.e. it works with the smallest kernel size in comparison to median or mean blurring types, which significantly affects calculation time. Symmetrical window of Gaussian Blurring is described by the following equation:

$$h(k,l) \rightarrow G(k,l) = \frac{1}{2\pi\sigma^2} e^{-\frac{k^2+l^2}{2\sigma^2}} \qquad (2)$$

where σ is standard deviation - parameter of applied distribution in x and y direction. In our case σ has the same value in both directions and it is calculated automatically as a function of window size K_{GB}, by equation described in OpenCV manual:

$$\sigma = 0.3 \cdot \left(\frac{K_{GB}-1}{2} - 1\right) + 0.8 \qquad (3)$$

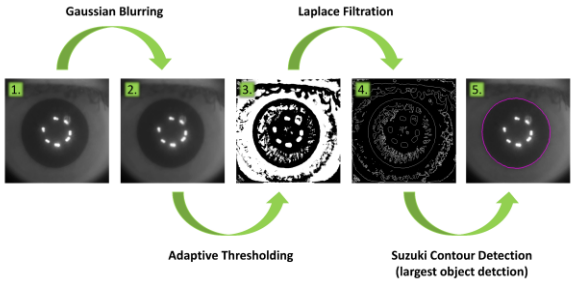

Fig. 2. Images of eye after each step of AED method. The original image: 1.; the image after Gaussian Blurring: 2.; the image after Adaptive Thresholding: 3.; the image after Laplace Edge Detection: 4; the original image with extracted biggest contour (magenta line) by Suzuki Contour Detection: 5. Sizes of Gaussian Blurring kernel and window of Adaptive Thresholding were set to 11 and 71, respectively.

Adaptive Thresholding of previously blurred image is second step of presented method. It is computationally more expensive than global thresholding by constant value, but it performs much better color binarization for non-homogenously illuminated images which are obtained sometimes by our optical set-up. Adaptive Thresholding binarizes the image, pixel by pixel. Local threshold for this binarization is computed as a weighted mean of pixels below the filtering window K_{AT}. Pixel weights are Gaussian kernel coefficients (2) with σ calculated from the equation (3) with K_{GB} substituted by K_{AT}.

Third step of the AED method is edges extraction from previously binarized image by calculating Laplacian with constant $h(k,l)$ aperture:

$$h(k,l) = \begin{pmatrix} 0 & 1 & 0 \\ 1 & -4 & 1 \\ 0 & 1 & 0 \end{pmatrix} \quad (4)$$

We set the smallest possible Laplacian aperture, because it results with edges of thickness of one pixel, thicker edges are unacceptable for the last step of our method.

The last step of extraction of precise pupil edge, is the Suzuki contour detection algorithm [10] - very useful and fast tool of algorithmic efficiency $O(width \cdot heigh)$. Next, we are calculating areas of all detected contours and choose the biggest one. We assume that edges of pupil are the biggest contour on image, which is true for most images obtained by our set-up.

V. Least Squares Circle Fitting

After detection of pupil edge coordinates on the image with size $W \cdot H$ pixels, we get the set of points $P(x_i, y_i)$ in $\mathbb{N}^2$ space, where values of $P(x_i, y_i) \in [0;\ 2^8 - 1 = 255]$ and $0 \leq i < N$. Extracted set of points, although forming pupil contour, is inconvenient for fast and simple computations e.g. radius, center coordinates and area. Therefore we fit analytically circle to the detected pupil edge by using Linear Least Square Method (LLSq).

We are fitting the circle to the constant number of M points, where $M < N$ is number of points selected for fitting. Obviously, total number of extracted points N differs between consecutive images, because pupil size and shape are not the same between frames. Our method of obtaining M is shown in Fig. 3: detected pupil contour is divided into M parts and median point of each portion of contour is chosen. Accordingly, we have the same number of points for fitting for every registered image or movie frame.

Linear Least Square method is probably the most popular one for fitting the functions to the dataset of points. It minimizes the sum of squared errors S, which is given by following formula for circle function:

$$S(u_c, v_c, R) = \sum_{i=1}^{N} [(u_i - u_c)^2 + (v_i - v_c)^2 - R^2]^2 \quad (5)$$

where u_c and v_c are coordinates of the central pixel in x and y direction, respectively. $u_i = x_i - < x >$ and $v_i = y_i - < y >$ are deviation coordinates describing position of pupil edge pixel in relation to the mean coordinate of all chosen M points and y directions.

If we want to minimize the sum of squared errors given by (5), we have to calculate derivatives:

$$\frac{\partial S(u_c, v_c, R)}{\partial u_c \partial v_c \partial R} = \left(\frac{\partial S}{\partial u_c}, \frac{\partial S}{\partial v_c}, \frac{\partial S}{\partial R}\right) = 0 \quad (6)$$

which for u_c and v_c it leads to the set of equations for obtaining the center of fitted pupil:

$$\begin{cases} u_c \underbrace{\sum_{i=1}^{N} u_i^2}_{a} + v_c \underbrace{\sum_{i=1}^{N} u_i v_i}_{b} = \underbrace{\frac{1}{2}\left(\sum_{i=1}^{N} u_i^3 + \sum_{i=1}^{N} u_i v_i^2\right)}_{d} \\ u_c \underbrace{\sum_{i=1}^{N} u_i v_i}_{b} + v_c \underbrace{\sum_{i=1}^{N} v_i^2}_{c} = \underbrace{\frac{1}{2}\left(\sum_{i=1}^{N} v_i^3 + \sum_{i=1}^{N} v_i u_i^2\right)}_{e} \end{cases} \quad (7)$$

Solution of above set of equations gives coordinates of fitted circle center:

$$\begin{cases} u_c = \frac{W_x}{W_r} \\ v_c = \frac{W_y}{W_r} \end{cases} \quad (8)$$

where $W_x = dc - be$, $W_y = e(a - b)$ and $W_r = ac - b^2$ and a, b, c, d, e are components of (7). Translation of coordinates by average position of all points forming pupil edge, gives position of center of fitted circle and approximated pupil center in the image:

$$(x_c, y_c) = (< x >, < y >) + (u_c, v_c). \quad (9)$$

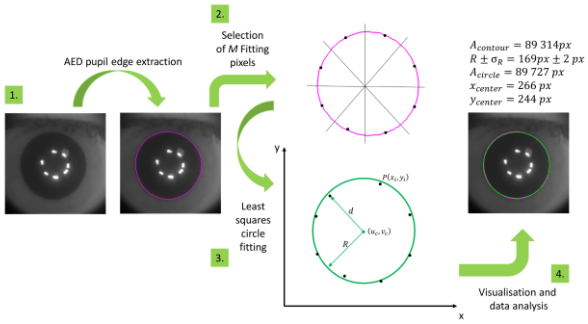

Fig. 3. Proposed method of fitting the circle to the detected pupil edge. Step 1. shows AED biggest contour extraction. Step 2 describes method of selecting M points for fitting presented on step 3. Black dots are median points of each part of contour after dividing it into M portions. Step 4 shows found pupil edge (magenta) and circle fitted to this edge (green) on the exemplary eye image.

The last derivative $\frac{\partial S}{\partial R}$ from (6) with obtained u_c and v_c coordinates gives square value of radius of fitted circle:

$$R^2 = {u_c}^2 + {v_c}^2 + \frac{1}{N}\left(\sum_{i=1}^{N} {u_i}^2 + \sum_{i=1}^{N} {v_i}^2\right) \quad (10)$$

VI. Haar Features Based Cascade Classifier Training

Presented AED method is efficient for images with pupil forming the biggest contour found by Suzuki algorithm. Presence of eyelashes, reflections of illuminator located near the pupil edge or reflections of stimulating beams sometimes lead to finding of incorrect contour on image and malfunction of AED method. To deal with this, we propose to use Hfbc classifier, which allows to detect objects after training of machine learning model by using positive and negative images, which do not contain the object of interest.

For training Hfbc classifier we created special collection of pupil-only images by cutting out, from the original ones, the area with found circle and resizing all of them to 64 px x 64 px. We have selected 1350 positive pupil-only images, additionally we have used 2700 negative images, without the pupil or even eyeball [26] and used them all for training Hfbc classifier [4]. Exemplary pupil-only images are shown in Fig. 4. They present pupils with four types of external illuminators. The pupil size is changing during stimulation, which causes that position of illuminator reflection in respect to the pupil edge is different between consecutive frames. Additionally, reflections of stimulation beams vary as well due to scanning. Training of Hfbc classifier on such prepared images was performed with all available Haar features available in OpenCV 4.0.1. Minimal hit rate set to 0.95 with Gentle

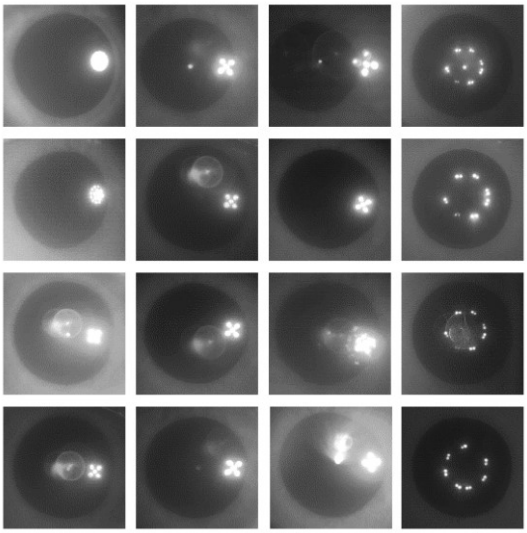

Fig. 4. Examples of positive training pupil-only images presents different types of used illuminators. Detected pupils were extracted with 20 px padding. All training images were rescaled to 64 px x 64 px.

AdaBoost boosting was enough to detect the pupil region from frames that exhibited malfunction of AED method.After training, our program is able to find pupil edge on images, for which it was failed with this before - two examples are shown in Fig. 5 and 6, obtained on series of images registered during two cases of two-photon vision tests. The biggest contours found by Suzuki algorithm are presented on small eye images in the upper rows a. of Fig. 5 and Fig. 6 by blue lines and it is clearly visible, that it does not follow the pupil edge. Consequently, the fitted circles obtained by LLSq (green lines) also substantially differ from real pupil. It is additionally depicted on upper plots (rows c.) on Fig. 5 and Fig. 6. by showing differences between pupil diameter of fitted circle (LsDA) and pupil diameter computed from area of biggest contour by Suzuki method (ADA) on the consecutive frames. After implementation and training of Hfbc classifier, the results are much better, which is presented on Fig. 5 and Fig. 6 in b. and d. rows. Cyan square shows pupil-only region detected by Hfbc classifier; blue and green lines (Suzuki contour and LLSq fitted circle, respectively) follow real edge of the pupil – Fig. 5 and 6, rows b. The differences between LsDA and ADA traces for consecutive frames are also minimal – Fig. 5 and 6, rows d. The plots presented on last rows e. of Fig. 5 and 6 show ratio between above two diameters: LsDA/ADA, whenever it equals one (or is relatively close to), it means the correct operation of our method.

So far we have collected database of ~100 thousands pupil images from our set-up and for ~10 thousand of them, pupil would not be detected properly without Hfbc classifier. In particular, this approach is very helpful for images with side illuminator reflections causing pupil border highly disturbed or even covered.

VII. Error analysis

Precision of pupil border detection method can be evaluated by basic statistics given by two below equations:

$$< d > = \frac{1}{N} \sum_{i=1}^{N} d_i, \qquad (11)$$

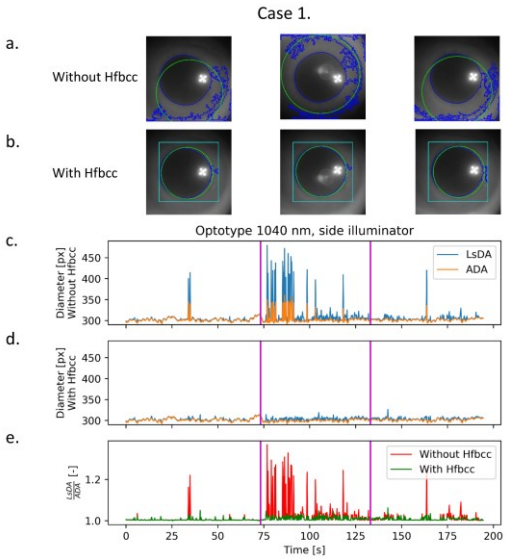

Fig. 5. First example of improvement of perfomance of our method after implementation trained Hfbc classifier. a.: before implementation Hfbc, biggest Suzuki contour - blue line, LLSq fitted circle – green line; b.: after training Hfbc, detected pupil-only region – cyan square, other lines the same as in a.; c.: before implementation Hfbc, diameters: of LLSq fitted circle (LsDA) – blue line and calculated from area of Suzuki contour (ADA) – orange line, for consecutive frames registered during experiment; d. after implementation of Hfbc: diameters of LLSq fitted circle – blue (LsDA) and Suzuki area diameter (ADA) – orange for consecutive frames; e.: ratio of LsDA and ADA before (red) and after (green) implementtion and training of Hfbc classifier.

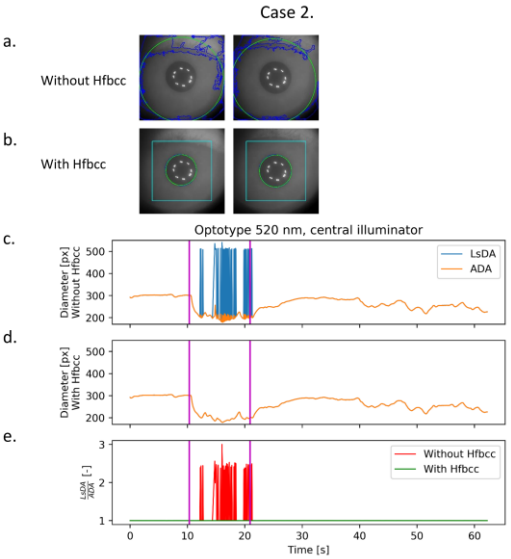

Fig. 6. Second example of improvement of perfomance of our method after implementation trained Hfbc classifier. a.: before implementation Hfbc, biggest Suzuki contour - blue line, LLSq fitted circle – green line; b.: after training Hfbc, detected pupil-only region – cyan square, other lines the same as in a.; c.: before implementation Hfbc, diameters: of LLSq fitted circle (LsDA) – blue line and calculated from area of Suzuki contour (ADA) – orange line, for consecutive frames registered during experiment; d. after implementation of Hfbc: diameters of LLSq fitted circle – blue (LsDA) and Suzuki area diameter (ADA) – orange for consecutive frames; e.: ratio of LsDA and ADA before (red) and after (green) implementtion and training of Hfbc classifier.

$$\sigma_R = \sqrt{\frac{1}{N-1}\sum_{i=1}^{N}(d_i - < d >)^2}, \qquad (12)$$

where $d_i = \sqrt{(x_c - x_i)^2 + (y_c - y_i)^2}$ is an Euclidean distance between detected pupil center and i'th border pixel, $< d >$ and σ_R describe average Euclidean distance and its standard deviation, respectively. Since we can assume that pupil is circle-like object, the distance $< d >$ given by equation (11) should be comparable with calculated from equation (10) radius R. For the properly detected edges, we can expect that distribution of distances d_i is narrow, so the standard deviation σ_R should be small. In principle it is possible that for incorrectly detected pupil edge pixels distribution of d_i results with $< d >$ value near to R. Therefore, only taking into account both above coefficients gives high reliability of proper pupil border detection.

For the cases with properly detected pupil, maximal value of σ_R reaches 10 pixels, e. g. on Fig. 3 where $\sigma_R = 2$px. For the other cases, with not precisely (or not at all) found pupil border, value of σ_R reaches more than 100 pixels, which is unacceptable because it is more than 50% error of calculated radius R. It can be observed in Fig. 5 and 6, rows a. Additionally, coefficients $< d >$ and σ_R can be used in post-processing for filtering out the failed images, e. g. registered during blinking.

VIII. Conclusions

In this paper we present the Adaptive Edge Detection method for extraction of precise coordinates forming pupil edge, which was designed and implemented in self-constructed instrument dedicated for two-photon vision examinations. Main advantage of our method is highly resistance to reflections of light sources e.g. pupil illuminators or stimulating laser beams. Additionally, it is easy to implement and has low computational complexity with approximated order of $O(width \cdot height)$. Main disadvantage of presented method was related with assumption, that the pupil is the biggest object on the image or in the area where AED method is applied. However, we handle with this problem by machine learning technique named Haar feature based cascade classifier. The machine learning model was previously trained on the set of specially prepared pupil-only images. Therefore, AED method is applied only to automatically detected region of the image consisted of pupil-only. After this improvement, our method is able to manage with images, for which it failed before implementation of Hfbc classifier. Finally, we are able to obtain pupil radius and central pixel coordinates, even for images containing eyelashes, changed position of illuminator or presence of reflections caused by stimulating laser beam.

References

[1] S. Uchida, "Image processing and recognition for biological images," *Dev. Growth Differ.*, vol. 55, no. 4, pp. 523–549, 2013. doi.org/10.1111/dgd.12054

[2] A. Krizhevsky, I. Sutskever, and G. E. Hinton, "mageNet Classification with Deep ConvolutionalNeural Networks" *Adv. Neural Inf. Process. Syst.*, pp. 1–9, 2012. doi.org/10.1145/3065386

[3] A. Kihm, L. Kaestner, C. Wagner, and S. Quint, "Classification of red blood cell shapes in flow using outlier tolerant machine learning" *PLoS Comput. Biol.*, vol. 14, no. 6, pp. 1–15, 2018. doi.org/10.1371/journal.pcbi.1006278

[4] V. Paul and J. Michael, "Rapid Object Detection using a Boosted Cascade of Simple Features" *IEEE*, vol. 1, pp. 511–518, 2001. doi.org/10.1109/CVPR.2001.990517

[5] L. Świrski, A. Bulling, and N. Dodgson, "Robust real-time pupil tracking in highly off-axis images" p. 173, 2012. doi.org/10.1145/2168556.2168585

[6] S. Ren, K. He, R. Girshick, and J. Sun, "Faster R-CNN: Towards Real-Time Object Detectionwith Region Proposal Network" *IEEE Trans. Pattern Anal. Mach. Intell.*, vol. 39, no. 6, pp. 1137–1149, 2017. doi.org/10.1109/TPAMI.2016.2577031

[7] R N Daschoudhary, "Real Time Face Detection and Tracking Using OpenCV" *Int. J. Res. Emerg. Sci. Technol.*, no. 4, 2017.

[8] G. Palczewska *et al.*, "Human infrared vision is triggered by two-photon chromophore isomerization" *Proc. Natl. Acad. Sci. U. S. A.*, vol 111, no. 50, pp. E5445-54, 2014 doi.org/10.1073/pnas.1410162111

[9] A. Zielińska, K. Kiluk, M. Wojtkowski, and K. Komar, "System for psychophysical measurements of two-photon vision" vol. 11, no. 1, pp. 1–3, 2019. doi.org/10.4302/plp.v11i1.837

[10] K. A. S.Suzuki, "Topological structural analysis of digital binary image by border following" *Cvgip*, vol. 30, pp. 32–46, 1985. doi.org/10.1016/0734-189X(85)90016-7

[11] F. D. Bremner, "Pupil assessment in optic nerve disorders" *Eye*, vol. 18, no. 11, pp. 1175–1181, 2004. doi.org/10.1038/sj.eye.6701560

[12] Y. J. Yoo, H. K. Yang, and J. M. Hwang, "Efficacy of digital pupillometry for diagnosis of Horner syndrome" *PLoS One*, vol. 12, no. 6, pp. 1–12, 2017. https://doi.org/ 10.1371/journal.pone.0178361

[13] W. Baumann, "Pupil Signs of Sympathetic Autonomic Neuropathy in Patients With Type 1" vol. 25, no. 9, 1998. https://doi.org/10.2337/diacare.25.9.1545

[14] D. Couret *et al.*, "Reliability of standard pupillometry practice in neurocritical care: An observational, double-blinded study" *Crit. Care*, vol.20, no.1, pp.1–9, 2016. https://doi.org/10.1186/s13054-016-1239-z

[15] L. F. Marshall, D. Barba, B. M. Toole, and S. A. Bowers, "The oval pupil: clinical significance and relationship to intracranial hypertension" *J. Neurosurg.*, vol. 58, no. 4, pp. 566–568, 1983. doi.org/10.3171/jns.1983.58.4.0566

[16] R. Chibel *et al.*, "Chromatic Multifocal Pupillometer for Objective Perimetry and Diagnosis of Patients with Retinitis Pigmentosa" *Ophthalmology*, vol. 123, no. 9, pp. 1898–1911, 2016. doi.org/10.1016/j.ophtha.2016.05.038

[17] D. Ben Ner *et al.*, "Chromatic pupilloperimetry for objective diagnosis of best vitelliform macular dystrophy" *Clin. Ophthalmol.*, vol. 13, pp. 465–475, 2019. doi.org/10.2147/OPTH.S191486

[18] G. Prabhakar and P. Biswas, "Eye Gaze Controlled Projected Display in Automotive and Military Aviation Environments" *Multimodal Technol. Interact.* vol. 2, no. 1, p. 1, 2018 doi.org/10.3390/mti2010001

[19] K. Murawski and K. Różanowski, "Pattern recognition algorithm for eye tracker sensor video data analysis" *Acta Phys. Pol. A*, vol. 124, no. 3, pp. 509–512, 2013. https://doi.org/10.12693/APhysPolA.124.509

[20] W. Fuhl, T. Kübler, K. Sippel, W. Rosenstiel, and E. Kasneci, "ExCuSe: Robust Pupil Detection in Real-World Scenarios" *Comput. Anal. Images Patterns*, vol. 9256, no. Chapter 4, pp. 39–51, 2015.

[21] W. Fuhl, T. C. Santini, T. Kuebler, and E. Kasneci, "ElSe: Ellipse Selection for Robust Pupil Detection in Real-World Environments" 2015. https://doi.org/10.1145/2857491.2857505

[22] J. Canny, "A computational approach to edge detection" *IEEE Trans. Pattern Anal. Mach. Intell.*, vol. 8, no. 6, pp. 679–98, 1986. https://doi.org/10.1109/TPAMI.1986.4767851

[23] T. Santini, W. Fuhl, and E. Kasneci, "PuRe: Robust pupil detection for real-time pervasive eye tracking" *Comput. Vis. Image Underst.*, vol. 170, pp. 40–50, 2018.

[24] R. Lienhart, A. Kuranov, V. Pisarevsky, and MRLT Report, "Empirical Analysis of Detection cascades of boosted classifiers for rapid object detection rainer" 2002.

[25] G. Bradski, "The OpenCV Library," *Dr. Dobb's J. Softw. Tools*, 2000.

[26] J. Deng, W. Dong, R. Socher, L.-J. Li, K. Li, and L. Fei-Fei, "ImageNet: A Large-Scale Hierarchical Image Database," in *CVPR09*, 2009.